AGU PUBLICATIONS

JGR

Journal of Geophysical Research: Atmospheres

RESEARCH ARTICLE

10.1002/2013JD020797

Key Points:
- Stratospheric equatorial waves extracted for the first time in coupled models
- Models produce realistic Kelvin and Rossby-gravity waves but with large spread
- Differences in resolution have more effects than differences in precipitation

Correspondence to:
F. Lott,
flott@lmd.ens.fr

Citation:
Lott, F., et al. (2014), Kelvin and Rossby-gravity wave packets in the lower stratosphere of some high-top CMIP5 models, *J. Geophys. Res. Atmos.*, *119*, 2156–2173, doi:10.1002/2013JD020797.

Received 26 AUG 2013
Accepted 17 JAN 2014
Accepted article online 23 JAN 2014
Published online 7 MAR 2014

Kelvin and Rossby-gravity wave packets in the lower stratosphere of some high-top CMIP5 models

F. Lott[1], S. Denvil[2], N. Butchart[3], C. Cagnazzo[4], M. A. Giorgetta[5], S. C. Hardiman[3], E. Manzini[5], T. Krismer[5], J.-P. Duvel[1], P. Maury[1], J. F. Scinocca[6], S. Watanabe[7], and S. Yukimoto[8]

[1]Laboratoire de Météorologie Dynamique, Ecole Normale Supérieure, Paris, France, [2]IPSL, Université Pierre et Marie Curie, Paris, France, [3]Met Office, Exeter, UK, [4]ISAC-CNR, Rome, Italy, [5]Max-Planck-Institut fur Meteorologie, Hamburg, Germany, [6]CCCMA, University of Victoria, Victoria, British Columbia, Canada, [7]Japan Agency for Marine-Earth Science and Technology, Yokohama Japan, [8]Climate Research Department, Meteorological Research Institute Tsukuba, Japan

Abstract We analyze the stratospheric Kelvin and Rossby-gravity wave packets with periods of a few days in nine high-top (i.e., with stratosphere) models of the fifth Coupled Model Intercomparison Project (CMIP5). These models simulate realistic aspects of these waves and represent them better than the tropospheric convectively coupled waves analyzed in previous studies. There is nevertheless a large spread among the models, and those with a quasi-biennial oscillation (QBO) produce larger amplitude waves than the models without a QBO. For the Rossby-gravity waves this is explained by the fact that models without a QBO never have positive zonal mean zonal winds in the lower stratosphere, a situation that is favorable to the propagation of Rossby-gravity waves. For the Kelvin waves, larger amplitudes in the presence of a QBO is counter intuitive because Kelvin waves are expected to have larger amplitude when the zonal mean zonal wind is negative, and this is always satisfied in models without a QBO. We attribute the larger amplitude to the fact that models tuned to have a QBO require finer vertical resolution in the stratosphere. We also find that models with large precipitation variability tend to produce larger amplitude waves. However, the effect is not as pronounced as was found in previous studies. In fact, even models with weak precipitation variability still have quite realistic stratospheric waves, indicating either that (i) other sources can be significant or that (ii) the dynamical filtering mitigates the differences in the sources between models.

1. Introduction

Kelvin and Rossby-gravity wave packets with periods of a few days dominate the day-to-day variability in the lower equatorial stratosphere. Such waves were first observed by *Wallace and Kousky* [1968] and *Yanai and Maruyama* [1966], and many studies have now documented their presence in vertical soundings or ground-based observations [*Tsuda et al.*, 1994; *Sassi et al.*, 2003; *Fujiwara et al.*, 2003], and using ultra-long duration balloons [*Vial et al.*, 2001; *Hertzog and Vial*, 2001]. These direct observations are today complemented by observations from meteorological satellites which provide a global description of the stratospheric equatorial waves (SEWs) [*Salby et al.*, 1984; *Randel and Gille*, 1991; *Mote et al.*, 2002; *Mote and Dunkerton*, 2004; *Alexander and Ortland*, 2010] and some of these satellite observations are now routinely assimilated in global models. This makes the SEWs quite well represented in meteorological analysis but significant errors still exist (for the European Centre for Medium-Range Weather Forecasts (ECMWF) analyses see *Ern et al.* [2008]). These errors likely explain that the different reanalysis available today present a large spread in their representation of the SEWs (at the tropopause level see *Fujiwara et al.* [2012]). As an illustration, the under estimation of wave activity in the ECMWF analysis found by *Ern et al.* [2008] that is mainly related to the Rossby-gravity waves, is still present in ERA-Interim [*Maury et al.*, 2013].

It is generally accepted that SEWs are largely forced by tropospheric convection [e.g., *Holton*, 1972; *Manzini and Hamilton*, 1993] and are partly related to the tropospheric convectively coupled equatorial waves (CCEWs) described by *Wheeler et al.* [2000] which travel coherently with convective centers in the troposphere [*Hendon and Wheeler*, 2008]. A clear example is given in *Maury et al.* [2013] where it is shown that SEWs are often present above CCEWs. Nevertheless, *Hendon and Wheeler* [2008] also show that the coherencies between equatorial waves and convection rapidly decrease with altitude because the CCEWs are rather slow. As a result their periods correspond to short vertical wavelength in the stratosphere where they dissipate rapidly. More recently, *Alexander and Ortland* [2010] have shown that the temporal variations of Kelvin wave activity in the tropical tropopause layer (TTL) and the stratosphere follows changes in propagation conditions (i.e., background winds and stability) rather than changes in Kelvin wave activity in convection.

Table 1. List of Models Used With Their Resolutions and Model Tops[a]

Name:	With Resolution	QBO Top	Kelvin	RG	Name:	Without Resolution	QBO Top	Kelvin	RG
(a) ERA-Interim (ERAI)	T255L60	10 Pa	–17 m/s	9 m/s	(b) MRI-CGCM3	T159L48	1 Pa	–5 m/s	–5 m/s
(c) MPI-MR	T63L95	1 Pa	–1 m/s	14 m/s	(d) MPI-LR	T63L47	1 Pa	–10 m/s	–11 m/s
(e) CMCC	T63L95	1 Pa	2 m/s	9 m/s	(f) IPSLCM5B	96 × 78 × L39	5 Pa	–9 m/s	–10 m/s
(g) HadGEM2-CC	192 × 144 × L60	1 Pa	–11 m/s	8 m/s	(h) IPSLCM5A	96 × 78 × L39	5 Pa	–10 m/s	–11 m/s
(i) MIROC-ESM	T42L80	0.3 Pa	–3 m/s	5 m/s	(j) CanESM2	128 × 64 × L35	1 hPa	–3.5 m/s	–4 m/s

[a]Also shown are the composite values of the zonal mean zonal wind corresponding to dates when Kelvin waves and Rossby-gravity waves are extracted to build the composites.

This dynamical filtering is also clearly apparent in *Flannaghan and Fueglistaler* [2013] which shows that the global wind fields induce a longitudinal mismatch between enhanced Kelvin wave activity in the TTL and in the Kelvin wave activity in tropospheric convection. Under favorable background flow conditions, this dynamical filtering can induce large SEWs even when the convection is not organized by CCEWs [*Garcia and Salby*, 1987] or when the sources are not the equatorial convection [*Maury and Lott*, 2013].

A large number of studies have analyzed the extent to which middle atmosphere General Circulation Models (GCMs) simulate SEWs [*Boville and Randel*, 1992; *Manzini and Hamilton*, 1993; *Amodei et al.*, 2001]. They show that GCMs can produce SEWs but that their amplitude is very sensitive to the convective parameterization used [*Horinouchi et al.*, 2003] and to vertical resolution in the stratosphere [*Boville and Randel*, 1992]. It is nevertheless difficult to evaluate if these models reproduce SEWs realistically, because the SEWs are modulated by the QBO [*Lott et al.*, 2009; *Yang et al.*, 2012] and the QBO was absent from most of the models used in *Horinouchi et al.* [2003]. Also, no studies have analyzed the SEWs in coupled models, where the interplay between convection and ocean surface temperature is taken into account more consistently than in GCMs forced with prescribed sea surface temperatures.

Because the significance of the stratosphere for the global climate is now well established, several Earth system models (ESMs) participating in the fifth Coupled Model Intercomparison Project (CMIP5) attempt to improve their representation of the stratosphere by extending their model higher and including the relevant additional physics. Among these models, four simulate a QBO: the Max-Planck Institute's medium resolution model MPI-MR [*Giorgetta et al.*, 2006], the Centro Euro-Mediterraneo per I Cambiamenti Climatici model with resolved stratosphere CMCC-CMS [*Manzini et al.*, 2012], the Met Office's model (Hadley Global Environment Model 2-Carbon Cycle) HadGEM2-CC [*Martin et al.*, 2011], and the JAMSTEC model for interdisciplinary research on climate MIROC-ESM [*Watanabe et al.*, 2011]. These models with a well represented stratosphere and a QBO have a large number of vertical levels (see Table 1), and also nonorographic gravity wave drag parameterization schemes. It is generally recognized that in these models the parameterized gravity waves contribute at least as much as the resolved waves to the QBO forcing [*Giorgetta et al.*, 2006]. In this sense they are consistent with early theories of the QBO [*Lindzen and Holton*, 1968] and with more recent observations [*Ern and Preusse*, 2009]. Some models for CMIP5 also have a reasonable stratosphere but vertical resolutions that are insufficient to simulate a QBO. In this paper, we will consider five of these models: the Meteorological Research Institute model MRI-CGCM3 [*Yukimoto et al.*, 2012], the Max-Planck Institute's model MPI-low resolution (LR), the two Institut Pierre-Simon Laplace (IPSL) models IPSL-CM5B and IPSL-CM5A [*Hourdin et al.*, 2013; *Dufresne et al.*, 2013], and the Canadian Center for Climate Modeling and Analysis model CanESM2 [*Arora et al.*, 2011; *von Salzen et al.*, 2013]. The total number of models considered is quite limited but it was considered desirable for the analysis to compare roughly the same number of models with and without a QBO. Another more practical constraint on the number of models used is the large amount of daily data required for the composite analysis.

Most of the studies that compare the SEWs between different stratospheric models are essentially based on spectral analysis [*Horinouchi et al.*, 2003; *Fujiwara et al.*, 2012] and provide little description of the spatiotemporal evolution of these waves. In this sense they are less comprehensive than the corresponding studies of CCEWs in the troposphere where characteristic patterns are often extracted via composite or regression techniques [e.g., *Straub et al.*, 2010]. Such techniques have been applied to SEWs in reanalysis data by *Lott et al.* [2009] or *Yang et al.* [2012] and allow to extract signals that compare very well in shape and amplitude with the unfiltered signals that modulate the day-to-day variability of the horizontal wind and temperature fields (compare for instance the temperature signal between unfiltered data during a given period and the

composite in *Lott et al.* [2009, Figures 3b and 4b]). For this comparison to make sense, the reconstruction has to take into account that the SEWs travel in packets with a finite time life cycle. All these aspects need to be sufficiently realistic to properly represent the breaking of the waves or their impact on dehydration. Also, spectral analysis can be misleading when focused on one process. For instance, if we are interested in the action of the wave on the zonal mean-flow by focusing on a spectral analysis of the Eliassen-Palm fluxes (as done in *Horinouchi et al.* [2003]), it may be concluded that a given model underestimates some waves. However, as shown in *Maury et al.* [2013] the same model can still have a realistic wave signature on other fields such as temperature, which is essential if we are interested in dehydration. More fundamentally, it is also important to verify that a spectral signature attributed to Kelvin waves in a given field, also has a pattern that corresponds to Kelvin wave packets when extracted and reconstructed.

The purpose of this paper is to conduct such spectral and composite analyses on a subset of models participating in CMIP5. First, a spectral analysis of tropospheric and stratospheric fields is made to evaluate the models' ability to reproduce CCEWs and SEWs. Second, a composite analysis of the waves is performed using the method introduced in *Lott et al.* [2009]. All results are presented according to the models ability to simulate the QBO and the precipitation variability.

2. Data Sets and Methodology

2.1. Data Sets

All the data used in this paper are from the nine ESMs which participated in CMIP5 and that were listed in the section 1 (see also Table 1). These nine models have a lid near or above the stratopause (around 1 hPa) and therefore include a stratosphere (see *Charlton-Perez et al.* [2013] for details), but they vary considerably in their horizontal and vertical resolution. Of these nine models, the four that simulate a QBO are also those with the largest number of levels in the vertical. In all the following figures these four models appear in the left column and the five models that do not simulate a QBO appear in the right column (following the order already given in Table 1). Note also that one model, the MRI-CGCM3 model, has a finer horizontal resolution than the other models. Note also that the CanESM2 model has a lid very close to the stratopause, significantly lower than in the other models, and this may affect the waves in the low stratosphere via reflections or damping near the model top. There are two models from the Max-Planck Institute which differ in terms of vertical resolution in the stratosphere and in the treatment of the ocean [*Giorgetta et al.*, 2013]. The high-resolution model (MPI-MR) simulates a QBO, whereas the low-resolution model (MPI-LR) does not [*Giorgetta et al.*, 2002]. The increased vertical resolution in MPI-MR could also help the model to more accurately simulate the vertical propagation of the waves. There are also two models from IPSL (IPSL5A and IPSL5B) that differ in their treatment of atmospheric turbulence, convection, and clouds [*Dufresne et al.*, 2013]. As a consequence, the IPSL5B model has a much stronger and more realistic precipitation variability in the tropics than IPSL5A. An advantage of the present study over previous studies on convective parameterization and stratospheric waves is that the two IPSL models differ only in few parameterizations (as in *Scinocca and McFarlane* [2004]), and the differences are such that the two models have realistic mean precipitation climatologies (they were both tuned for participation in CMIP5).

For each model we take the daily fields from the simulations covering the 50 years 1950–2000. The precipitation and the wind (u, v) on the 850hPa level are used to characterize the variability in the lower troposphere and the temperature and winds on the 50 hPa level to characterize the waves in the lower stratosphere. For validation, we will use the daily data from the GPCP data sets [*Adler et al.*, 2003] for precipitation and from the ERAI reanalysis [*Dee et al.*, 2011] for all the other fields. For ERAI we will consider 30 years (1980–2010) and for GPCP 13 years (1997–2010).

2.2. Methodology

To analyze the equatorial waves and their relation to convection we begin by following *Wheeler and Kiladis* [1999] and *Hendon and Wheeler* [2008] among others, and make space-time spectra of tropical signals. For precipitation, the spectra are displayed using an energy conserving formalism with log-axis and are superimposed on the spectral squared coherencies between the dynamical fields and the precipitation fields: these two techniques allow us to highlight the tropospheric CCEWs without needing to normalize the spectra with red-noise backgrounds [see *Hendon and Wheeler*, 2008]. On top of this, and following *Lott et al.* [2009] or *Maury et al.* [2013], we will analyze spectra of fields which are first tapered by a cosine function centered at the equator and crossing the zero line at $\pm 10^o$ and then averaged over the latitudinal band

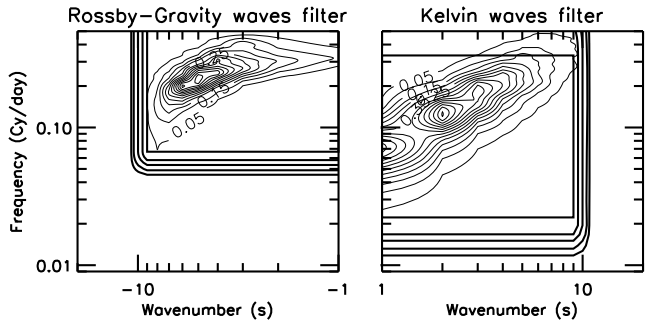

Figure 1. (left) Westward component of the 50 hPa spectra of the meridional wind (thin solid) and transfer function used to extract the Rossby-gravity waves (thick solid, contour interval=0.2). (right) Eastward component of the 50 hPa spectra of the zonal wind and transfer function used to extract the Kelvin waves. For all models the filters are identical but the spectra shown here are from ERAI data. To estimate the spectra, the fields are tapered in latitude by a cosine taper of 20^o width centered at the equator and then averaged in latitude over the equatorial band. Each year a time-longitude periodogram is then made and the spectra is estimated by averaging the periodograms over the years. The estimate of the spectra is further smoothed by applying 30 times a 1-2-1 filter in the temporal domain. This smoothes the signal over around 15 points, yielding a spectral resolution of around 4.10^{-2}cy/d.

(10^oS–10^oN). We will also compute spectra of anti-symmetric precipitations by simply replacing the cosine taper with a sine taper of the same width before averaging in latitude.

Example spectra from ERAI at 50 hPa are shown in Figure 1 (further details on the method are given in the figure caption). Figure 1 (left) shows the westward part of meridional wind (v) symmetric spectrum and Figure 1 (right) shows the eastward part of zonal wind (u) symmetric spectrum. The relative broadband maxima in these two panels are the signatures of the Rossby-gravity waves and of the Kelvin waves, respectively [*Lott et al.*, 2009].

To characterize the spatial structure and the life cycle of the SEWs we follow *Lott et al.* [2009] and make a composite analysis of band-pass filtered fields. For the Kelvin waves, the band-pass filter operates in the frequency-wave number Fourier space, by multiplying the Fourier components of all fields by the transfer function shown in Figure 1 (right). In this figure, we see that the filter largely contains the broadband spectral maxima associated with Kelvin waves in ERAI, which guarantees that the filtered fields include them well. To finalize the filtering we then return to physical space. To diagnose when a Kelvin wave is present at 50 hPa, we evaluate an index whose value equals the maximum of the filtered zonal wind averaged in latitude between 10^oS and 10^oN and identify the longitude λ_M at which this maximum occurs. The composites are centered on the λ_Ms and built from averages over dates when maxima of this index exceed a given threshold. In each data set the threshold is chosen so that around one event every 2 years is selected. We choose here to select a rather low number of events to guarantee independence between the selected wave packets, bearing in mind that each wave packet can have a life cycle that lasts near a month. Since this number is rather small, we have verified that none of our results are affected by moderate changes in the thresholds, provided that about the same number of dates are selected in each model (not shown). For the Rossby-gravity waves, we follow the same procedure but use the transfer function in Figure 1 (left) to build the band-pass filter and use the meridional wind v to define the index.

Figure 2 shows the indices for Kelvin waves and Rossby-gravity waves, together with the temporal evolution of the zonal mean zonal wind at 50 hPa. The Kelvin wave signal in zonal wind can exceed 10 m/s in some models (black lines), and the Rossby-gravity signal in the meridional wind can exceed 5 m/s (grey line). Some models show signals that are larger than in the reanalysis (Figure 2a), but it is important to recall that in the reanalysis fields the equatorial waves can be underestimated [*Ern et al.*, 2008] and can vary a lot from one reanalysis to the other (at 100 hPa, see *Fujiwara et al.* [2012]). Another interesting fact is that these signals vary from one model to the other and are substantially modulated by the QBO (see Figures 2a, 2c, 2e, 2g, and 2i). There is a tendency, in models that simulate a QBO and in ERAI, to produce a larger Kelvin wave index when the QBO at 50 hPa is westward, and a larger Rossby-gravity wave index when the QBO is eastward. As a consequence the composite method in the models with a QBO tends to pick dates when the QBO is westward/eastward at 50 hPa for Kelvin/Rossby-gravity waves (see *Lott et al.* [2009] and the composite values for the zonal mean zonal wind at 50 hPa in Table 1).

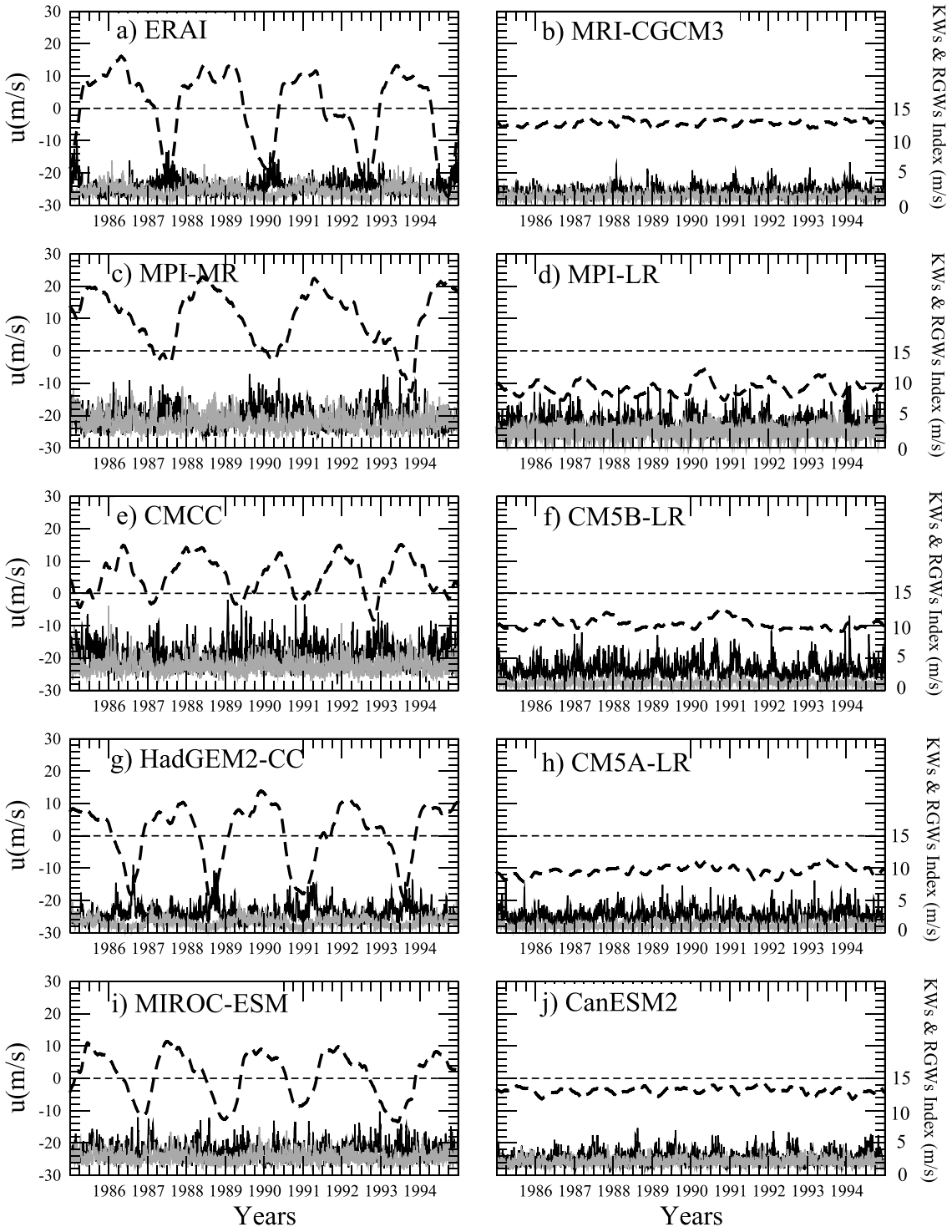

Figure 2. Zonal mean zonal wind at the Equator (dashed), Kelvin wave index (black), and Rossby-gravity waves index (grey). All series are built from 50hPa fields.

3. Kelvin Waves

3.1. Spectral Analysis

3.1.1. Precipitation and Tropospheric Winds

Spectra from the symmetric precipitations are presented in Figure 3. The first five models capture quite well the magnitude of the variability of both the westward and eastward directions (Figures 3b–3f). The remaining four models in this figure (Figures 3g–3j) underestimate this magnitude. Among the five

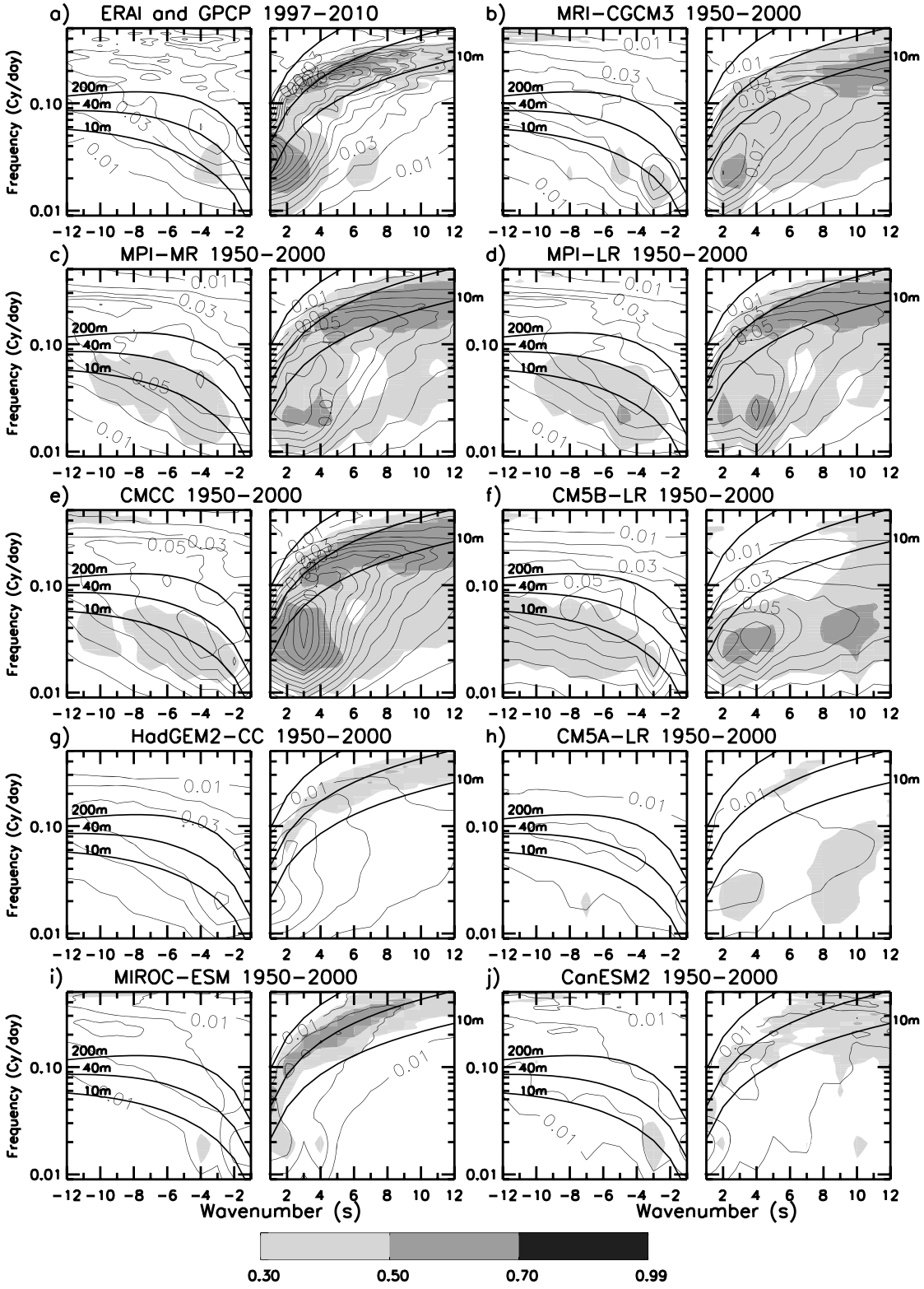

Figure 3. Spectra of symmetric precipitation (contour lines with interval=0.01 mm^2day^{-3}) and of its squared coherency with the zonal wind at 850 hPa (shaded). The precipitation and wind are first tapered by a cosine function of 20^o width centered at the equator and averaged over (10^oS–10^oN) before their frequency-wave number periodograms are evaluated. The squared coherencies are then built from ratio between cross-spectra and spectra, those being estimated from averaged and smoothed yearly periodograms and cross periodograms exactly as described in Figure 1. All the coherency levels shown are above the 99% level (which is around 0.2 for $r = 50$ degrees of freedom). In all figures are also shown the dispersion curves for the $n = 1$ Rossby waves and Kelvin waves with equivalent depths $h = 10, 40, 200$m.

models with quite realistic variability, four (Figures 3b–3d and 3i) also have relative maxima in the precipitation spectra that are near the dispersion curves of the equatorial Kelvin waves (thick solid lines on the right panels of Figures 3a–3j). In these four models, these relative maxima are also near where the coherency between the zonal wind at 850 hPa and the precipitation are quite large: they represent quite well both the convectively coupled Kelvin waves and the overall precipitation variability. Among these four models, three show very similar structure of the precipitation variability (Figures 3c–3e), which naturally follows that they share an ECHAM-based atmospheric component. This is quite interesting in that it offers an opportunity to isolate differences that come from the treatment of the stratosphere alone. One of the models with large precipitation variability has almost no contribution from the CCEWs to its variability (Figures 3f).

Among the four models with insufficient variability (Figures 3g–3j), two have some signature of CCEWs (Figures 3g and 3i) and two have little or no CCEWs (Figures 3h and 3j). Finally, it is useful to note that the IPSL model CM5B-LR has large precipitation variability and small convectively coupled Kelvin waves in Figure 3f, whereas the IPSL model CM5A-LR in Figure 3h has weak precipitation variability and weak convectively coupled waves. This is also interesting in that it offers an opportunity to isolate differences that come from the precipitation variability alone.

To summarize, we find a lot of contrast between different models' ability to simulate convectively coupled Kelvin waves, which is consistent with the CMIP3 analysis of *Straub et al.* [2010]. We also find a lot of difference in their ability to represent the overall variance of precipitation. Note again that in Figure 3 the models are classified in order of decreasing precipitation variability from top to bottom, after placing the models with a QBO on the left, and those without on the right. This is also the order that was already adopted in Table 1 and that we will keep all along the paper.

3.1.2. Stratospheric Wind

To identify the spectral domain in which Kelvin waves modulate the lower stratosphere the spectra for the zonal wind at 50 hPa are shown in Figure 4. In it we see that all the spectra have substantial power with well defined maxima in both the eastward and westward directions. In the westward direction, we know from *Lott et al.* [2009] that a good part of the signal is due to the free planetary waves and is therefore related to the extratropics. We will not discuss this further. In the eastward direction all models have substantial signatures of Kelvin waves, with larger amplitude for models with a QBO. For presentation purposes, the contour interval has been made 4 times larger in the eastward panels for models with a QBO (Figures 4c, 4e, 4g, and 4i). The essential role of QBO filtering is illustrated by noting that, of the models with a QBO, the smallest stratospheric Kelvin wave signal (Figure 4g) still has more Kelvin wave power than the model with the largest Kelvin wave signal in the group of models without a QBO (Figure 4d). When we look also from top to bottom, we see that the models with larger precipitation variability tend to have larger amplitude Kelvin waves in the stratosphere. Nevertheless, the differences between models are far less pronounced than their differences in terms of precipitation variability, which somehow mitigates the results in *Horinouchi et al.* [2003].

With respect to the influence of the precipitation variability, two factors suggest that the large-scale organization of convection by the CCEWs matters. First, the two models in Figures 4f and 4h have almost identical stratospheric Kelvin waves, whereas their differences in precipitation variability are very large (Figures 3f and 3h). As they both underrepresent the CCEWs this suggests that differences in precipitation variability only matters if they occur in a spectral domain that is not too far from that of the stratospheric Kelvin waves. For this to occur, having CCEWs certainly helps. Second, the models with QBO in Figures 4g–4i have quite substantial stratospheric Kelvin waves and quite small precipitation variability. This variability is nevertheless quite well placed between the dispersion curves corresponding to the CCEWs (Figures 3g–3i).

3.2. Composite Analysis

To characterize the spatial structure of Kelvin-wave life cycles, Figure 5 presents longitude-time composites of the zonal wind at the equator. It is seen that all models simulate substantial eastward propagating disturbances with wind maxima often reaching 5 m/s and more. Models with a QBO have a stronger Kelvin wave signal, and this signal moves faster eastward than in the reanalysis and in the models without a QBO. If we return to the zonal mean zonal winds and the 50 hPa Kelvin wave indexes in Figure 2, or to the zonal mean zonal wind composite values in Table 1, these excessively fast waves in the models with a QBO seem to be a consequence of the fact that these models tend to have an eastward bias. That is, during the dates

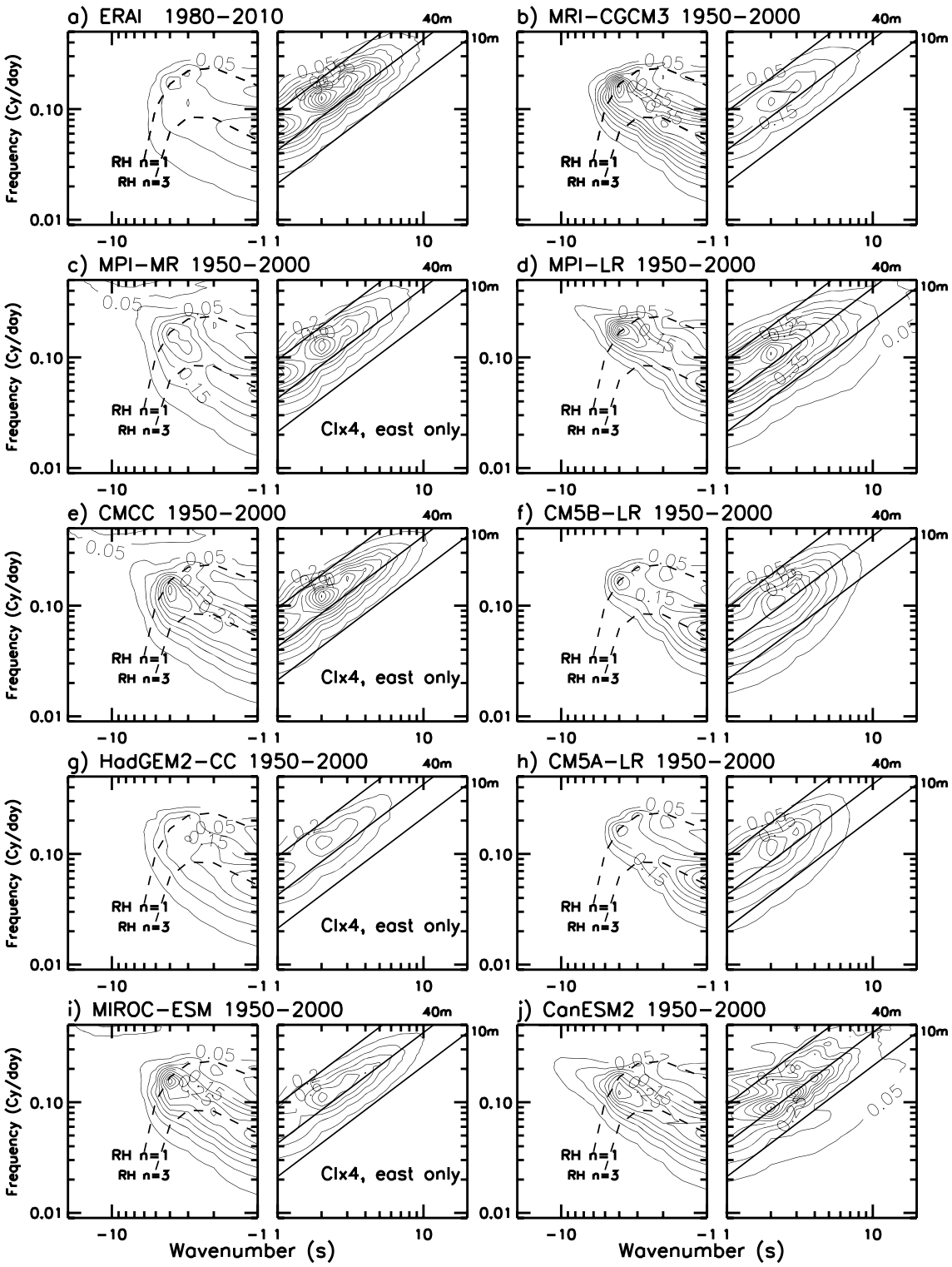

Figure 4. Spectra of the zonal wind at 50hPa tapered and averaged over the equatorial band as described in Figure 1 (contour interval: $0.05 m^2 s^{-2} day^{-1}$). The thick solid lines are for the Kelvin waves dispersion curves, whereas the dashed lines are for the free planetary waves dispersion curves with $n = 1, 3$ after application of a Doppler spread by an eastward wind $U = 15$m/s to take into account advection by the midlatitude winds.

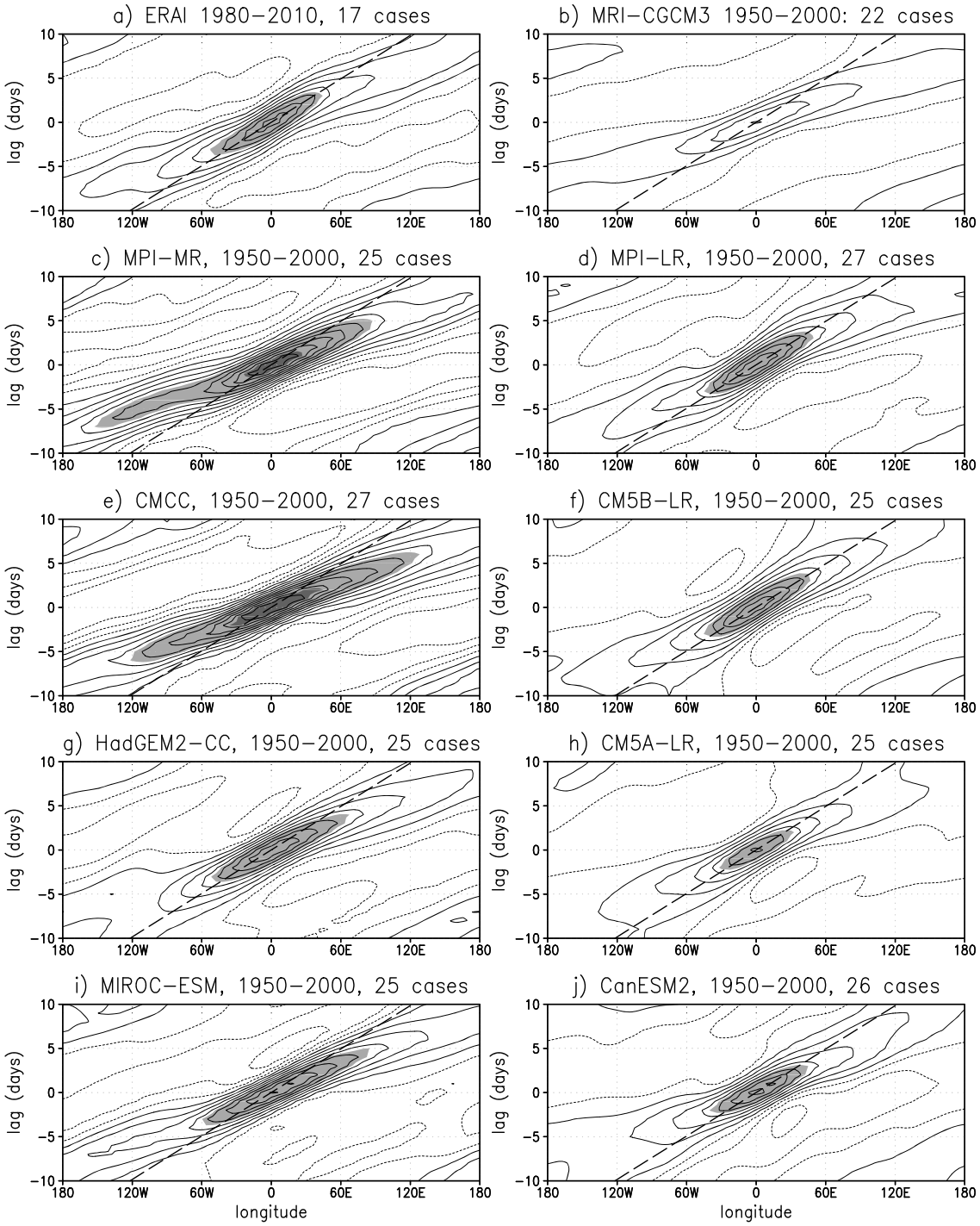

Figure 5. Time evolution of the zonal wind anomaly at the equator due to the passage of Kelvin waves at 50 hPa, contour interval: 1.25 m/s, values above 5 m/s and 10 m/s are in light grey and in dark grey respectively. The thick dashed line is for a uniform displacement at 15 m/s.

selected to build the composite, the zonal wind is larger (more eastward) than in the models with no QBO and in ERAI (see Table 1). In contrast, in the models without a QBO, the wave signal moves at about the same phase speed as in ERAI. This is because in these models the zonal mean zonal wind at the equator is always westward and with values near the observed values of the zonal mean zonal wind in the westward QBO phase (remember that in ERAI the dates selected to build the composite are essentially during westward QBO phase, Table 1).

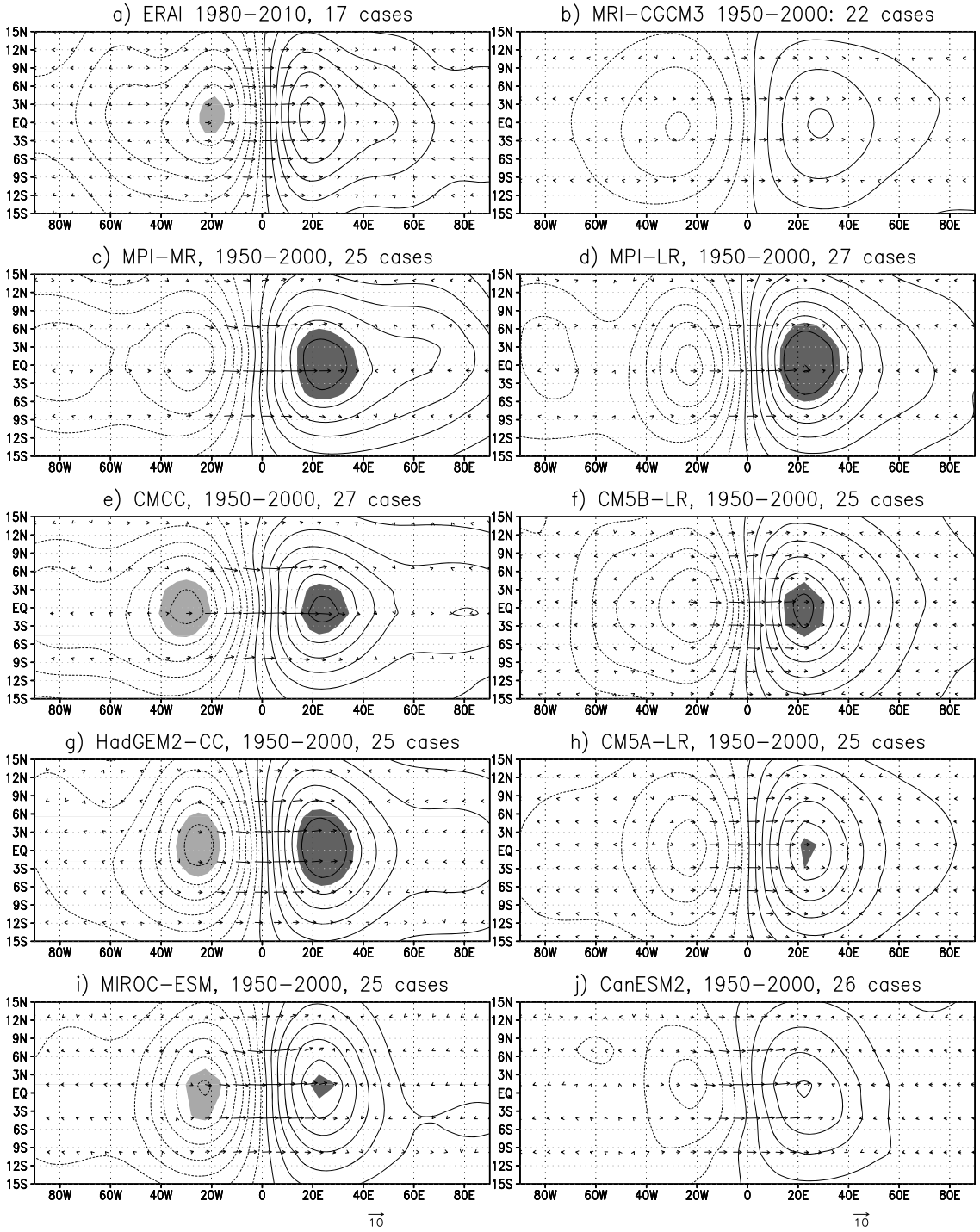

Figure 6. Composite maps of winds and temperature anomalies due to Kelvin waves at 0 day lag and at 50 hPa. The contours are for the temperature with contour interval = 0.75K and with values below −3 K and above 3 K light shaded and dark shaded, respectively. A value of 10 m/s for the wind arrows is indicated by the arrows below Figures 6i and 6j, and is identical for all panels.

These differences of phase speed in the stratosphere are consistent with the linear Kelvin wave theory in that waves with higher intrinsic phase speeds have larger vertical wavelengths and can propagate better vertically. In models with a QBO, the 50 hPa winds during the selected events are more eastward than in ERAI or in models without a QBO (see the fourth column in Table 1). Therefore, the 50 hPa Kelvin waves in the models with a QBO need to have larger horizontal phase speeds to result in the same vertical propagation

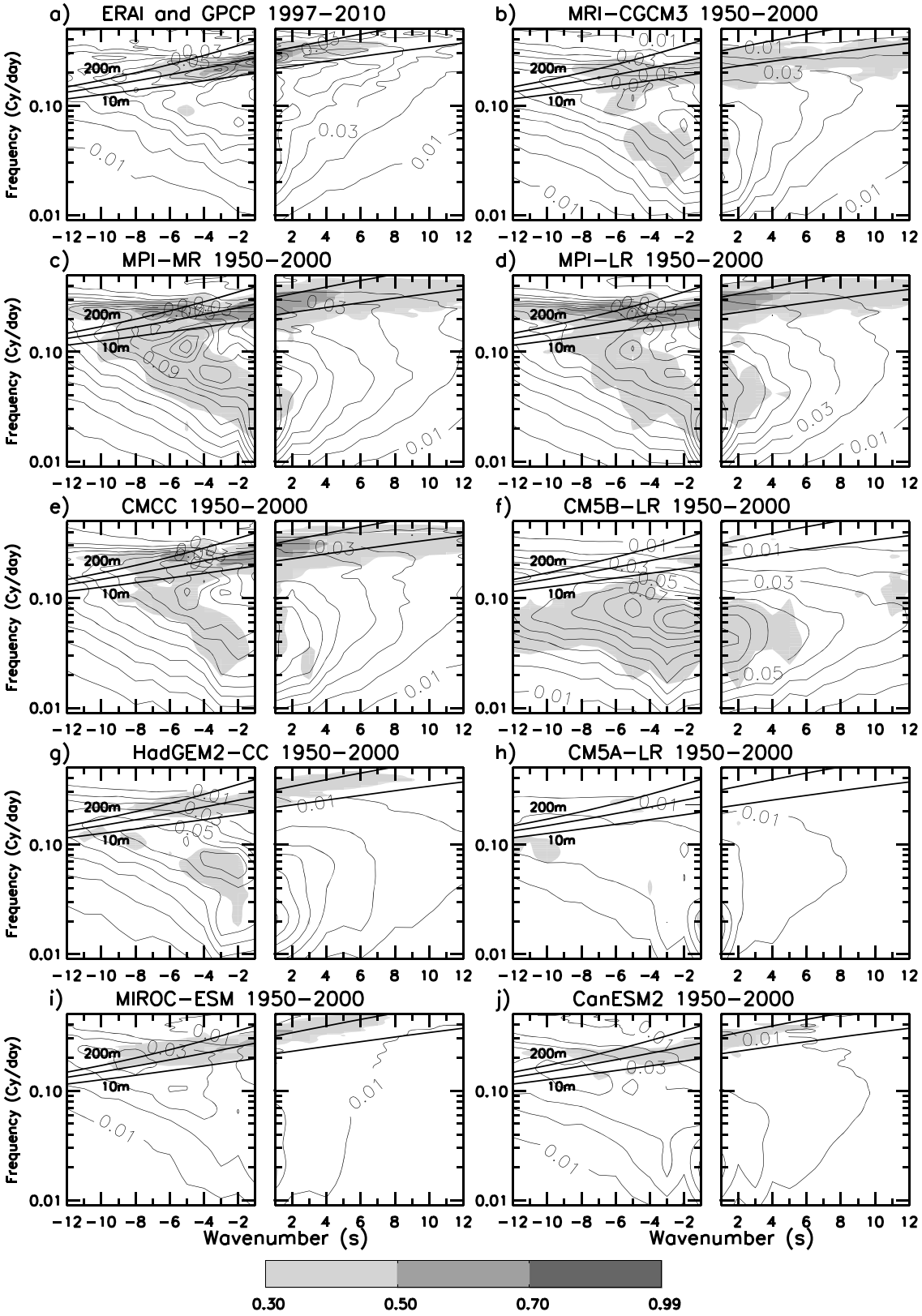

Figure 7. Spectra of antisymmetric precipitations (contour lines, interval 0.01mm^{2}day^{-3}) and squared coherency with the meridional wind at 850 hPa (shading). To build spectra and coherencies, the periodograms and cross-periodograms are evaluated from meridional wind fields averaged over the equatorial band as in Figure 1. The antisymmetric precipitation is estimated by multiplying the precipitation field by a sin taper of 20^o width centered at the equator and then averaged in latitude over (10^{o}S–10^{o}N). In all figures also the dispersion curves are shown for Rossby-gravity waves with $h = 10, 40, 200$m.

conditions as ERAI. In other words, the Kelvin waves with low phase speed have dissipated more in the models with a QBO because their intrinsic phase speed is lower than in the models without a QBO.

The winds and temperature composites at 0 day lag in Figure 6 confirm that we are well in the presence of Kelvin waves, with the disturbance horizontal wind being zonal and in quadrature with the temperature. Again, we see that the signal in temperature is quite substantial, reaching more than 3 K. An interesting fact is that in amplitude the temperature signals are quite identical when we compare models with a QBO and models without. This is somehow in contradiction with the differences in zonal winds between models in Figure 5 and cannot simply be explained by a Doppler effect. In fact, from linear wave theory, since the zonal wind and temperature fields due to Kelvin waves are both proportional to the geopotential divided by the intrinsic phase speed, the amplitude of the temperature signal should vary as that of the zonal wind.

Finally, it is also worth mentioning here that the two models in Figures 5b and 5j stand out from the others in the sense that they have quite small Kelvin waves signals. The first is characterized by its very fine horizontal resolution and the second by its rather low top.

4. Rossby-Gravity Waves

4.1. Spectral Analysis

4.1.1. Precipitation and Tropospheric Winds

The spectra of antisymmetric precipitation also differ between models (Figure 7). As for the symmetric precipitations in Figure 3, the first five models presented in this figure (Figures 7b–7f) have substantially larger variabilities than the four others. These five models also have larger variability than is observed (Figure 7a), and this was not the case for the symmetric spectra. This difference between the symmetric and antisymmetric results indicates that the simulated precipitation field is "whiter" than observed, and that the first five models have a tendency to produce a less organized precipitation variability at the large scale. This lack of large-scale organization is further indicated by the fact that the GPCP spectrum in Figure 7a has a well defined relative maximum between the dispersion curves of the Rossby-gravity waves, and where the coherency with the meridional wind at 850 hPa is also quite high. This indicates that convectively coupled Rossby-gravity waves organize a substantial part of the precipitation variability. This behavior is not well simulated by the models. On the one hand, a good part of them have enhanced coherency between precipitation and winds as indicated by the shaded zones between the dispersion curves for Rossby-gravity waves in Figures 7b–7e. On the other hand these enhanced coherencies do not correspond to relative maxima in the precipitation spectra. This indicates that, while there is some interactions between precipitation and dynamics in the Rossby-gravity wave spectral domain of the models, these interactions do not contribute to the precipitation variability as much as suggested by the observations.

As for the symmetric precipitation, we also find that for the model with large precipitation variability in Figure 7f the large scale waves do not contribute much to the variability. In the two models with quite low precipitation variability (Figures 7g and 7i) signatures of CCEWs are present, as indicated by the enhanced coherencies in the spectral domain of the Rossby-gravity waves.

4.1.2. Stratospheric Winds

At 50 hPa, models with a QBO have much more meridional wind variability than those without a QBO (Figure 8, where for presentation purpose the contour interval used for the three models with a QBO in Figures 8c, 8e, and 8i has been made 4 times larger than the contour interval used in the other models). In all the models with a QBO (Figure 8c, 8e, 8g, and 8h), the relative maxima are quite well located near the dispersion curves of the Rossby-gravity waves, and in agreement with ERAI in Figure 8a. In the models without a QBO, the relative maxima are either too small in amplitude (Figures 8b, 8f, and 8h) or clearly in error in terms of location and shape (Figures 8d and 8j). Again, from top to bottom, the differences between the meridional wind spectra in part follows from differences in convection variability. Here we say "in part" because this result is only clear when we compare the models with a QBO in the Figures 8c and 8e to the models without a QBO in Figures 8g and 8h. For the models without a QBO, the differences in the stratospheric spectra seem to be unrelated to differences in convection variability.

4.2. Composite Analysis

The maps in Figure 9 present longitude time-section of the composites of meridional wind at the equator. They show that all the models simulate westward propagating disturbances that shift continuously toward the east as expected for westward Rossby-gravity waves having eastward group velocity. As expected from the spectra, the waves have much larger amplitude and are more realistic in the models with a QBO than

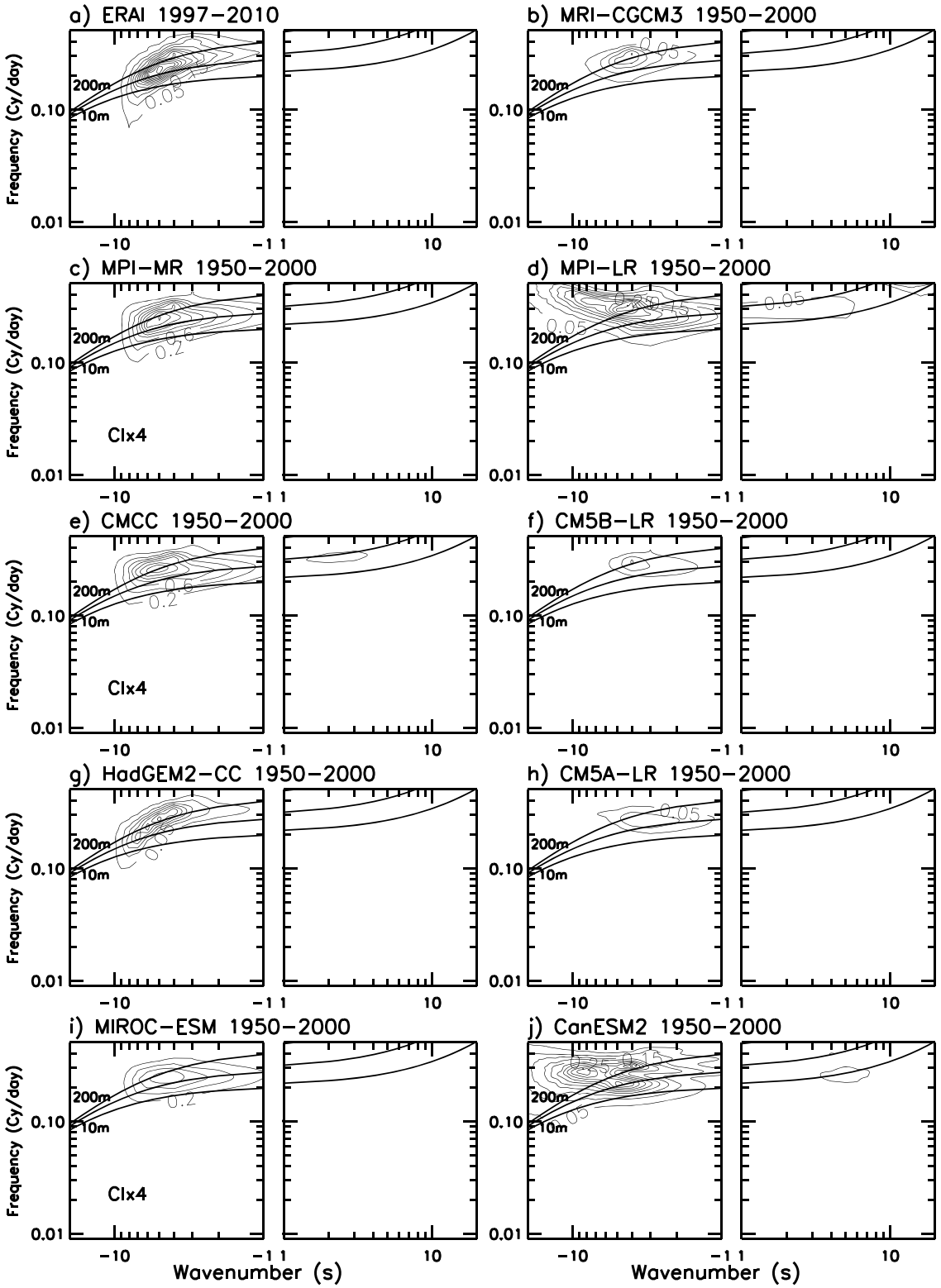

Figure 8. Spectra of the meridional wind at 50 hPa and averaged over the equatorial band (contour interval: 0.05m^{2}s^{-2}day^{-1}).

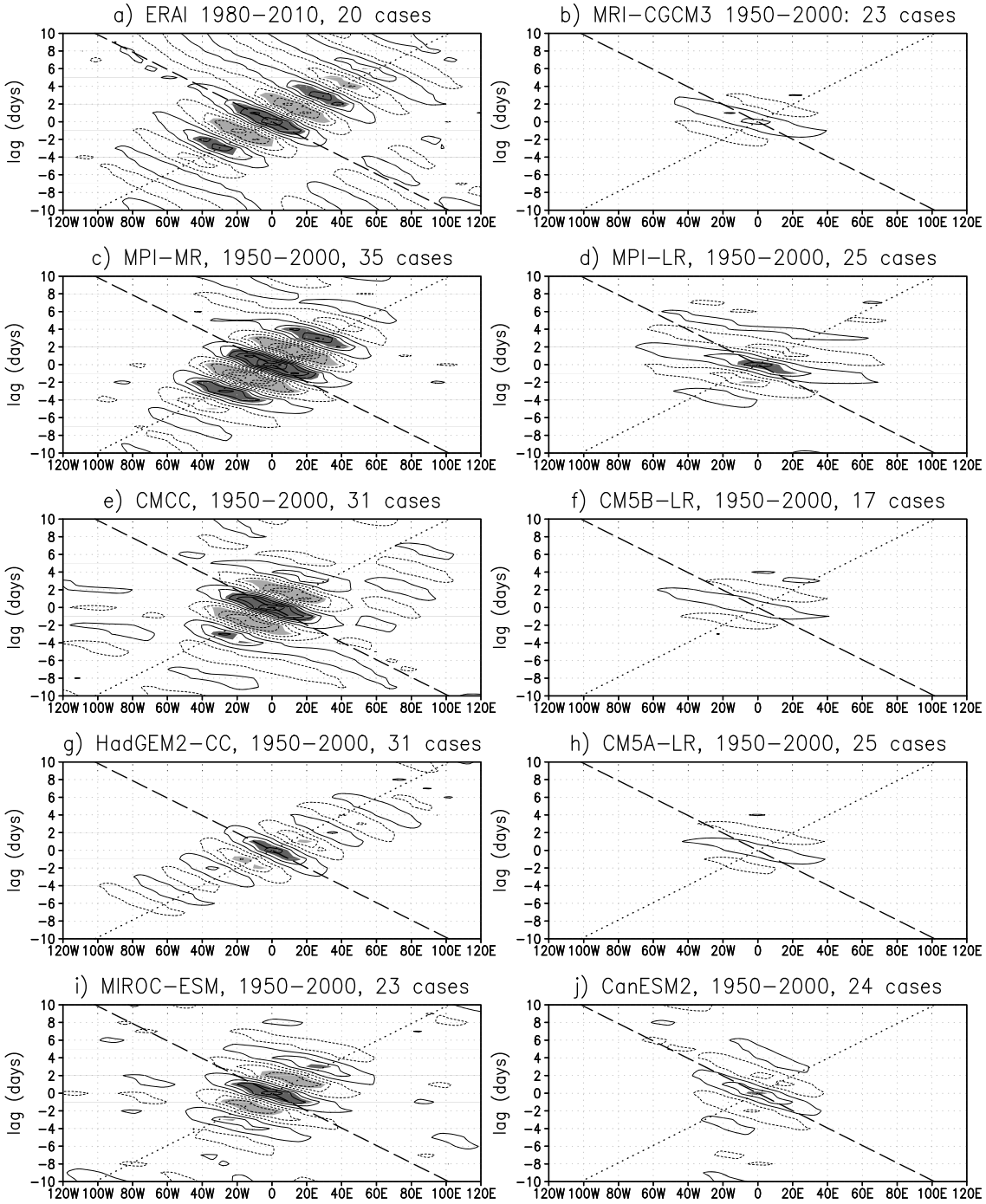

Figure 9. Time evolution of the meridional wind anomaly at the equator due to the passage of Rossby-gravity waves at 50 hPa, contour interval=1 m/s, values below −2 m/s and above 2 m/s are grey shaded and dark shaded, respectively. The dotted and dashed lines are for horizontal displacement at the speeds of ±13 m/s, respectively.

without. Again a sensitivity to convection is only apparent in the models with a QBO, with larger amplitude waves in the two models in Figures 9c and 9e than in the two models in Figures 9g and 9i. What seems more remarkable in Figure 9 are the large differences in propagation characteristics. In most of the models the disturbances tend to have a much larger and negative phase speed than is seen in the observations, where it is near −13 m/s (compare the phase lines slope to the dashed line). There is one exception, Figure 9g where the disturbance propagates at about the observed phase speed indicated in Figure 9a. Consistent with these differences, the groups of waves in the models propagate more slowly eastward than in ERAI, except again

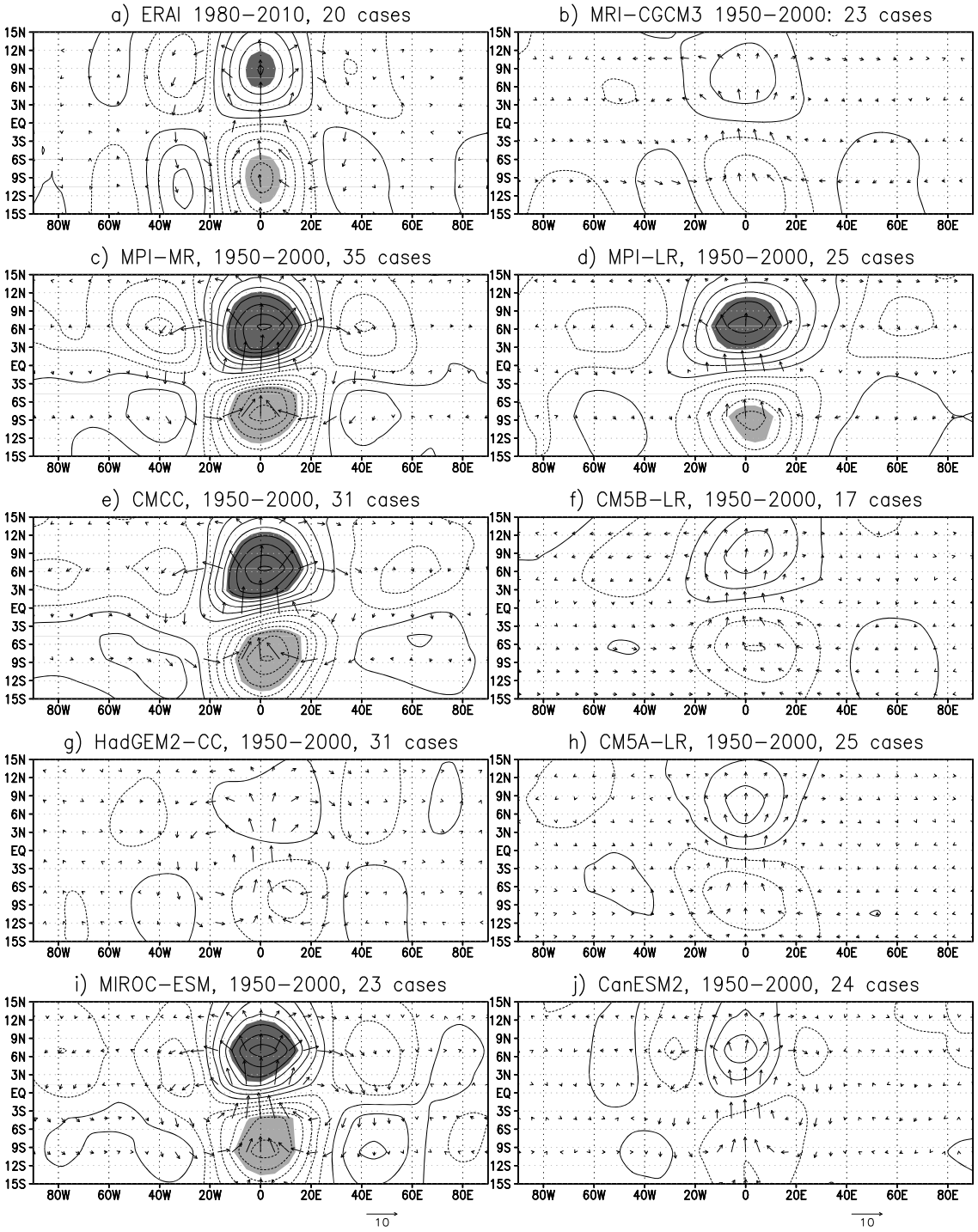

Figure 10. Composite maps of winds and temperature for the Rossby-gravity waves at 0 day lag and at 50 hPa. Contour Interval 0.25K, values below -1K and above 1K are grey shaded and dark shaded, respectively. A value of 10 m/s for the wind arrows is indicated by the arrows below the lower two panels and is identical for all panels.

for the model in Figure 9g where they propagate slightly faster (in all subfigures compare the amplitude displacement of the group of waves to the dotted lines). Note that this relatively fast group propagation in the model of Figure 9g can not be explained in terms of stronger advection by the background wind since the composite zonal mean zonal wind of about +8 m/s (see Table 1) in this model is not much different from the composite zonal mean zonal wind found in the other models with a QBO. This slow eastward propagation bias in all but one QBO model becomes very pronounced when one looks to the models without

a QBO. In these models the meridional wind oscillations almost stay confined within the same longitude bands as time evolves (Figures 9b, 9d, 9f, 9h, and 9i).

The composite maps for horizontal wind and temperature in Figure 10 confirm that we are in presence of Rossby-gravity waves. The amplitude reach more than 1 K in temperature for most models with a QBO (Figures 10c, 10e, and 10i), except again for the model in Figure 10g where it is much smaller. It is also interesting that the signal in the models with a QBO is substantially larger than the signal in the reanalysis (except again for the model in Figure 10g). Finally, it seems that the two models with a QBO and stronger convection variability (Figures 10c and 10e) have larger wave amplitudes than the two with weaker convection variability (Figures 10g and 10i). Nevertheless, this interpretation should be taken with care, since the model in Figure 10g behaves here quite differently from the others, and since the model in Figure 10i has a quite reasonable Rossby-gravity waves signal. For the models without a QBO there are still coherent Rossby-gravity waves structures and this occurs despite the fact that the zonal mean zonal wind is negative in all of them (see Table 1). This inherently yields a small amplitude intrinsic phase speed and hence more efficient vertical dissipation. Still in the models without a QBO the effect of convection variability is hard to detect, and this is particularly evident when we compare the two IPSL models in Figures 10f and 10h again.

5. Conclusion

According to the subset of CMIP5 simulations considered in this paper, the simulation of the precipitation variability is still a major issue. More precisely, the spectral distribution of the precipitation variability and the contribution of the CCEWs to this variability differ significantly between models (Figures 3 and 7). In this sense, the situation is not much better than for the models participating in CMIP3 and analyzed for instance in *Straub et al.* [2010]. As we are here mostly interested in the stratosphere, this should impact the stratospheric waves according to *Horinouchi et al.* [2003], and partly because the convectively coupled Kelvin waves can emit substantial Kelvin waves in the stratosphere [*Maury et al.*, 2013].

Despite these differences, most of the nine models have substantial and quite realistic Kelvin waves and some Rossby-gravity waves in the lower stratosphere. This shows that the relation between the stratospheric waves and the convection is more subtle than expected, suggesting that convection is not the only source of waves and that the dynamical filterings by the zonal wind and by the vertical resolution largely mitigate the differences between the models in terms of precipitation.

In general the models have little difficulties in simulating stratospheric Kelvin wave packets because these waves have a quite large vertical wavelength and a positive phase speed. In models without a QBO their propagation is favored by the fact that the zonal mean zonal wind is very often negative, which results in large intrinsic phase speed and large vertical wavelength. In models with a QBO this situation is only met roughly half of the time. Nevertheless, and despite the fact that the favorable conditions for the Kelvin wave propagation are less frequent in models with a QBO, we find that the models with a QBO have larger amplitude Kelvin waves than the models without (Figure 4). The explanation of this apparent contradiction could be that the refined vertical resolution in the lower stratosphere needed to produce a QBO also helps to better resolve the Kelvin waves. A good illustration is the comparison between the two MPI models that only differ by their resolution in the stratosphere: the one with a QBO and refined vertical resolution has a stronger Kelvin wave signal than the other (Figures 5c and 5d). This sensitivity of the Kelvin waves to the vertical resolution is probably one of the causes that models need such refined resolutions to produce a QBO. While it has been found that models without a QBO underestimate the stratospheric Kelvin waves, it must also be noted that some models without a QBO have about the right Kelvin wave signal in temperature and only underestimate the signal in zonal wind.

For Rossby-gravity waves, the differences between the models are much more pronounced than for Kelvin waves. For instance models without a QBO tend to produce very fast westward propagating Rossby-gravity waves. In fact in these models, the Rossby-gravity waves must have negative phase speeds that are inferior to the negative zonal mean zonal wind (see for instance the spectra in Figure 8d, or the composites in Figures 9b, 9d, 9f, 9h, and 9j). Also, the positive intrinsic group speed of the waves opposed the advection by the negative zonal mean zonal wind, and the Rossby-gravity wave packets tend to stay at the same place (Figures 9b, 9d, 9f, 9h, and 9j) instead of moving eastward (Figure 9a). Of course, many of the models without a QBO have problems in producing these waves coherently as illustrate the composites presented in Figures 10b, 10d, 10f, 10h, and 10j. For models with a QBO, the Rossby-gravity waves are much better

represented (see Figures 9 and 10) but there are big qualitative and quantitative differences between the models. In three models with a QBO, the Rossby-gravity waves have excessively strong westward phase speed but excessively weak eastward group speeds, while maintaining quite large amplitudes.

It emerges from this discussion that models differ significantly in their ability to represent large scale Kelvin and Rossby-gravity wave packets in the lower stratosphere. Nevertheless, these differences are less related to the variability of convection than we would have expected from earlier papers [*Horinouchi et al.*, 2003]. This conclusion should nevertheless be moderated by the fact that we have only analyzed here large scale waves. They are, however, consistent with more recent observational papers which show that the climatology of the wave activity in the tropical tropopause layer is not closely related to the tropospheric convection [*Alexander and Ortland*, 2010]. The differences between the models seem to be controlled more by the vertical resolution [*Boville and Randel*, 1992]. This probably follows that (i) the models with refined vertical scales likely induce less numerical dissipation of the vertically propagating waves (this is quite evident for the Kelvin waves), and that (ii) the models with high vertical resolution also have a QBO and simulate better the background wind conditions favorable to these waves (this is quite clear for the Rossby-gravity waves). The fact that vertical resolution is really a crucial issue is further illustrated by the two models presented in panels (b) and (j) of Figures 10–10. These two models have problems in representing the large-scale equatorial waves, one is characterized by a quite high horizontal resolution, the other by a top that is quite low (at the stratopause).

Finally, our result that the influence of convection is not as large as we could have expected from past studies should be tempered by the fact that we did not look at the vertical distribution of the latent heating associated with precipitation and we know since *Holton* [1972] that this factor is essential to the efficiency of wave forcing. Also, the weak sensitivity to convection we found in the two IPSL models, which only differ by their treatment of the convection parameterization in the atmosphere, could well be due to that the two versions lack of convective variability near the spectral domain of the SEWs. It would therefore be very helpful to compare twin models that only differ in their representation of the CCEWs. In fact, even if CCEWs in part dissipate before reaching the stratosphere, their presence is certainly beneficial to inject coherent structure on the variabilities of precipitations at the large horizontal spatial scales and rather fast time scales of the Kelvin and Rossby-gravity wave packets that propagate in the stratosphere.

Acknowledgment
This work was supported by the European Commission's 7th Framework Programme, under the projects EMBRACE (grant agreement 282672) and COMBINE (grant agreement 226520), and by the ANR project STRADYVARIUS. GPCP Precipitation data are provided by the NOAA/OAR/ESRL PSD, Boulder, Colorado, USA, from their Web site at http://www.esrl.noaa.gov/psd/. S. Watanabe was supported by the SOUSEI program, MEXT, Japan, and his simulations were performed using the Earth Simulator.

References

Amodei, M., S. Pawson, A. A. Scaife, U. Langematz, W. Lahoz, D. M. Li, and P. Simon (2001), The SAO and Kelvin waves in the EuroGRIPS GCMS and the UK Met. Office analyses, *Ann. Geophys.*, *19*, 99–114, doi:10.5194/angeo-19-99-2001.

Adler, R. F., et al. (2003), The Version 2 Global Precipitation Climatology Project (GPCP) monthly precipitation analysis (1979–Present), *J. Hydrometeor.*, *4*, 1147–1167.

Alexander, M. J., and D. A. Ortland (2010), Equatorial waves in High Resolution Dynamics Limb Sounder (HIRDLS) data, *J. Geophys. Res.*, *115*, D24111, doi:10.1029/2010JD014782.

Arora, V. K., J. F. Scinocca, G. J. Boer, J. R. Christian, K. L. Denman, G. M. Flato, V. V. Kharin, W. G. Lee, and W. J. Merryfield (2011), Carbon emission limits required to satisfy future representative concentration pathways of greenhouse gases, *Geophys. Res. Lett.*, *38*, L05805, doi:10.1029/2010GL046270.

Boville, B. A., and W. J. Randel (1992), Equatorial waves in a stratospheric GCM: Effects of the vertical resolution, *J. Atmos. Sci.*, *9*, 785–801.

Charlton-Perez, A. J., et al. (2013), On the lack of stratospheric dynamical variability in low-top versions of the CMIP5 models, *J. Geophys. Res. Atmos.*, *118*, 2494–2505, doi:10.1002/jgrd.50125.

Dee, D. P., et al. (2011), The ERA-Interim reanalysis: Configuration and performance of the data assimilation system, *Q. J. R. Meteorol. Soc.*, *137*, 553–597, doi:10.1002/qj.828.

Dufresne, J.-L., et al. (2013), Climate change projections using the IPSL-CM5 Earth System Model: From CMIP3 to CMIP5, *Clim. Dyn.*, *40*(9-10), 2123–2165, doi:10.1007/s00382-012-1636-1.

Ern, M., P. Preusse, M. Krebsbach, M. G. Mlynczak, and J. M. Russell (2008), Equatorial wave analysis from SABER and ECMWF temperatures, *Atmos. Chem. Phys.*, *8*, 845–869.

Ern, M., and P. Preusse (2009), Quantification of the contribution of equatorial Kelvin waves to the QBO wind reversal in the stratosphere, *Geophys. Res. Lett.*, *36*, L21801, doi:10.1029/2009GL040493.

Flannaghan, T. J., and S. Fueglistaler (2013), The importance of the tropical tropopause layer for equatorial Kelvin wave propagation, *J. Geophys. Res. Atmos.*, *11*, 5160–5175, doi:10.1002/jgrd.50418.

Fujiwara, M., M. K. Yamamoto, H. Hashiguchi, T. Horinouchi, and S. Fukao (2003), Turbulence at the tropopause due to breaking Kelvin waves observed by the Equatorial Atmosphere Radar, *Geophys. Res. Lett.*, *30*(4), 1171, doi:10.1029/2002GL016278.

Fujiwara, M., J. Suzuki, A. Gettelman, M. I. Hegglin, H. Akiyoshi, and K. Shibata (2012), Wave activity in the tropical tropopause layer in seven reanalysis and four chemistry climate model data sets, *J. Geophys. Res.*, *117*, D12105, doi:10.1029/2011JD016808.

Garcia, R. R., and M. L. Salby (1987), Transient response to localized episodic heating in the tropics. Part II: Far-field behavior, *J. Atmos. Sci.*, *44*, 499–530.

Giorgetta, M. A., E. Manzini, and E. Roeckner (2002), Forcing of the quasi-biennial oscillation from a broad spectrum of atmospheric waves, *Geophys. Res. Lett.*, *29*(8), 86-1–86-4, doi:10.1029/2001GL014756.

Giorgetta, M. A., E. Manzini, E. Roeckner, M. Esch, and L. Bengston (2006), Climatology and forcing of the quasi-biennial oscillation in the MECHAM5 model, *J. Clim.*, *19*, 3882–3901.

Giorgetta, M. A., et al. (2013), Climate and carbon cycle changes from 1850 to 2100 in MPI-ESM simulations for the Coupled Model Intercomparison Project phase 5, *J. Adv. Model. Earth Syst.*, *5*(3), 572–597, doi:10.1002/jame.20038.
Hendon, H. H., and M. C. Wheeler (2008), Some space-time spectral analyses of tropical convection and planetary-scale waves, *J. Atmos. Sci.*, *65*, 2936–2948.
Hertzog, A., and F. Vial (2001), A study of the dynamics of the equatorial lower stratosphere by use of ultra-long-duration balloons 2: Gravity waves, *J. Geophys. Res.*, *106*, 22,745–22,761.
Hourdin, F., et al. (2013), Impact of the LMDZ atmospheric grid configuration on the climate and sensitivity of the IPSL-CM5A coupled model, *Clim. Dyn.*, *40*(9-10), 2197–2192, doi:10.1007/s00382-012-1411-3.
Holton, J. R. (1972), Waves in the equatorial stratosphere generated by tropospheric heat sources, *J. Atmos. Sci.*, *29*, 368–375.
Horinouchi, T., S. Pawson, K. Shibata, E. Manzini, M. A. Giorgetta, F. Sassi, R. J. Wilson, K. Hamilton, J. DeGrandpe, and A. A. Scaife (2003), Tropical cumulus convection and upward propagating waves in middle-atmospheric GCMs, *J. Atmos. Sci.*, *60*, 2765–2782.
Lindzen, R. S., and J. R. Holton (1968), A theory of the quasi-biennial oscillation, *J. Atmos. Sci.*, *25*, 1095–1107.
Lott, F., J. Kuttippurath, and F. Vial (2009), A climatology of the gravest waves in the equatorial Lower and middle stratosphere: Method and comparison between the ERA-40 re-analysis and the LMDz-GCM, *J. Atmos. Sci.*, *66*, 1327–1346.
Manzini, E., and K. Hamilton (1993), Middle atmospheric traveling waves forced by latent and convective heating, *J. Atmos. Sci.*, *50*, 2180–2200.
Manzini, E., C. Cagnazzo, P. G. Fogli, A. Bellucci, and W. A. Muller (2012), Stratosphere-troposphere coupling at inter-decadal time scales: Implications for the North Atlantic Ocean, *Geophys. Res. Lett.*, *39*, L05801, doi:10.1029/2011GL050771.
Martin, G. M., et al. (2011), The HadGEM2 family of Met Office Unified Model Climate configurations, *Geosci. Model Dev. Discuss.*, *4*, 765–841, doi:10.5194/gmdd-4-765-2011.
Maury, P., and F. Lott (2013), On the presence of equatorial waves in the lower stratosphere of a general circulation model, *Atmos. Chem. Phys. Discuss.*, *13*, 22,607–22,637, doi:10.5194/acpd-13-22607-2013.
Maury, P., F. Lott, L. Guez, and J.-P. Duvel (2013), Tropical variability and stratospheric equatorial waves in the IPSLCM5 model, *Clim. Dyn.*, *40*, 2331–2344, doi:10.1007/s00382-011-1273-0.
Mote, P. W., T. J. Dunkerton, and D. Wu (2002), Kelvin waves in stratospheric temperature observed by the Microwave Limb Sounder, *J. Geophys. Res.*, *107*(D14), ACL 10-1–ACL 10-10, doi:10.1029/2001JD001056.
Mote, P. W., and T. J. Dunkerton (2004), Kelvin wave signatures in stratospheric trace constituents, *J. Geophys. Res.*, *109*, D03101, doi:10.1029/2002JD003370.
Randel, W. J., and J. C. Gille (1991), Kelvin wave variability in the upper stratosphere observed in SBUV ozone data, *J. Atmos. Sci.*, *48*, 2330–2349.
Salby, M. L., D. L. Hartmann, P. L. Bailey, and J. C. Gille (1984), Evidence for equatorial Kelvin modes in NIMBUS-7 LIMS, *J. Atmos. Sci.*, *41*, 220–235.
Sassi, M. N., et al. (2003), A study of equatorial wa583 ves characteristics using rockets, balloons, Lidar and Radar, *Adv. Space Res.*, *5*, 813–818, doi:10.1016/S0273-1177(03)00412-5.
Scinocca, J. F., and N. A. McFarlane (2004), The variability of modelled tropical precipitation, *J. Atmos. Sci.*, *61*, 1993–2015.
Straub, K. H., P. T. Haertel, and G. N. Kiladis (2010), An analysis of convectively coupled Kelvin waves in 20 WCRP CMIP3 global coupled climate models, *J. Clim.*, *23*, 3031–3056.
Tsuda, T., Y. Murayama, H. Wiryosumarto, S. W. B. Harijono, and S. Kato (1994), Radiosonde observations of equatorial atmosphere dynamics over Indonesia, 1: Equatorial waves and diurnal tides, *J. Geophys. Res.*, *99*, 10,591–10,516.
Vial, F., A. Hertzog, C. R. Mechoso, C. Basdevant, P. Cocquerez, V. Dubourg, and F. Nouel (2001), A study of the dynamics of the equatorial lower stratosphere by use of ultra-long-duration balloons 1: Planetary scales, *J. Geophys. Res.*, *106*, 22,725–22,743.
von Salzen, K., J. F. Scinocca, N. A. McFarlane, J. Li, J. N. S. Cole, D. Plummer, M. C. Reader, X. Ma, M. Lazare, and L. Solheim (2013), The Canadian Fourth Generation Atmospheric Global Climate Model (CanAM4). Part I: Physical processes, *Atmos. Ocean*, *51*, 104–125, doi:10.1080/07055900.2012.755610.
Wallace, J. M., and V. E. Kousky (1968), Observational evidence of Kelvin waves in the tropical stratosphere, *J. Atmos. Sci.*, *25*, 900–907.
Watanabe, S., et al. (2011), MIROC-ESM 2010: Model description and basic results of CMIP5-20c3m experiments, *Geosci. Model Dev.*, *4*, 845–872, doi:10.5194/gmd-4-845-2011.
Wheeler, M., and G. N. Kiladis (1999), Convectively coupled equatorial waves: Analysis of clouds and temperature in the wavenumber-frequency domain, *J. Atmos. Sci.*, *56*, 375–399.
Wheeler, M., G. N. Kiladis, and P. J. Webster (2000), Large-scale dynamical fields associated with convectively coupled equatorial waves, *J. Atmos. Sci.*, *57*, 613–640.
Yang, G.-Y., B. Hoskins, and L. Gray (2012), The influence of the QBO on the propagation of equatorial waves into the stratosphere, *J. Atmos. Sci.*, *69*, 2959–2982, doi:10.1175/JAS-D-11-0342.1.
Yanai, M., and T. Maruyama (1966), Stratospheric wave disturbances in the tropical stratosphere, *J. Meteorol. Soc. Jpn*, *44*, 291–294.
Yukimoto, S., et al. (2012), A new global climate model of the Meteorological Research Institute: MRI-CGCM3-Model description and basic performance, *J. Meteorol. Soc. Jpn*, *90A*, 23–64, doi:10.2151/jmsj.2012-A02.